Torregrosa, AJ.; Broatch, A.; Quintero-Igeño, P.; Redondo-Navarro, ÁR.; Morin, F. (2022). Assessment of the fluid-dynamic and acoustic behaviour of a swirl static mixer for after-treatment systems. Applied Acoustics. 186:1-9. https://doi.org/10.1016/j.apacoust.2021.108446

Assessment of the fluid-dynamic and acoustic behaviour of a swirl static mixer for after-treatment systems

A. J. Torregrosa, A. Broatch, P. Quintero, Á. Redondo

CMT - Motores Térmicos. Universitat Politècnica de València (Spain).

F. Morin

Renault (France).

Abstract

An investigation on the acoustic transmission loss and the pressure drop caused by a mixer inducing element located downstream of the Diesel Exhaust Fluid (DEF) injection point was carried out in order to reduce the knowledge gap identified for this kind of after-treatment system elements. Transmission Loss measurements were performed at 4 mass flow rate conditions; 0, 100, 200 and 300 kg/h. Additionally, pressure drop measurements were registered for a range of mass flow rates, from 0 to 800 kg/h at steps of 50 kg/h, with similar flow and room temperatures. The post-processing and analysis included the application of a decomposition technique in the case of the transmission loss, which lead to understand the contribution of reflective and dissipative effects to the total attenuation. Reference results, for the particular geometry and kind of mixer element characterized is provided, as well as the full extent of the analysis of the results and the insights of the decomposition analysis technique, and different modeling possibilities have been explored. The conclusions indicate that, while usually overlooked, these devices may have a significant influence on the exhaust acoustics, either due to the possibility of occurrence of flow noise generation, or to the influence of their presence on the attenuation of the aftertreatment device as a whole.

Keywords: Mixer Element, After-treatment Systems, Pressure Drop, Transmission Loss, Reflective and Dissipative Decomposition

1. Introduction

The current trend to tighten emission regulations is constantly pushing research and development efforts into improving engine performance and enhancing palliative after-treatment systems (ATS) [1, 2]. The broad use of Diesel engines with their collateral NOx problems have consolidated Selective Catalytic Reduction (SCR) systems as a usual solution [3] and one of the most favorable to be used [4]. This technology was first used in industrial stationary

applications, and then was transferred to mobile applications starting with the marine sector, and since 2005 approximately in automotive applications, with the respective challenges on the designing for function and integration within the vehicle/engine package [5].

SCR systems are among the ATS technologies that require certain chemical species to be injected into the exhaust system. For instance, active diesel particulate filters (DPF) require some fuel to be injected for regeneration to take place, likewise the diesel exhaust fluid (DEF), also known as urea-water solution (UWS), is injected in SCR systems for NOx reduction [2]. The two most relevant points to guarantee a proper and efficient SCR functioning are the urea injection and the mixing [4]: injecting the right amount at any given operating conditions is key to avoid insufficient NOx reduction due to lack of, or unacceptably high ammonia slip due to excess. On the other hand, uniform flow distribution and mixing of reductant with exhaust gases must be ensured to achieve the desired high NOx conversion. Maldistribution can also induce poor NOx conversion and ammonia slip in specific channels, even simultaneously [6]. Designing and tuning the trade-off between NOx conversion efficiency and Ammonia Slip is challenging [3].

The flow maldistribution problem can be reduced by means of avoiding upstream flow disturbances (e.g. elbows), but placing mixers (mixing inducers) and sufficient pipe length upstream of the SCR catalyst are the most common solutions [2]. A good level of ammonia, and reaching good homogeneity after the injection into the main exhaust gas flow and before it reaches the catalyst inlet, can be achieved by means of turbulence induction, flow fragmentation, setting a complex path for the fluid or simply leaving a longer time and space for the species to mix [4].

The specific shape, structure or geometry of the mixers is often referred to as embodiment, and determines the way it interacts with the flow. Usual types include: swirl inducing mixers [7, 8, 9] with stator vanes sprouting from the outside to the center, with the orientation of each blade to induce swirling movement; lateral line tabs to divide streamlines [10, 11, 12], perforated plates [13]; wire-mesh-like wall structure [14], and spiral passages [2]. Some solutions make use of different combinations, such as wire-mesh and baffle sections [15], straight and twisted tabs over a unified fluid-guiding body [16], or perforated spiral guiding tabs followed by another to baffles, one spiral inducing and another perforated, systematically forcing the flow to spin and to divide streamlines [17]. Some of these embodiments are illustrated in Figure 1.

There is a relatively abundant literature on the mixing efficiency and the pressure drop, as well as on the use of numerical modeling, specially CFD, to approach these studies. Related studies involving both experimental measurements alongside to numerical simulation, date back to Seo *et al.* in 2008, who studied the effects of blade characteristics of a swirl mixer on the fluid mixing [20], and are still an active field, as shown by the recent contributions of Zhang *et al.* [21], Blinov *et al.* [22] and Zhao *et al.* [23].

In contrast, no research regarding nor mentioning the acoustic influence or the Transmission Loss (TL) of the mixer element has been found, and thus it

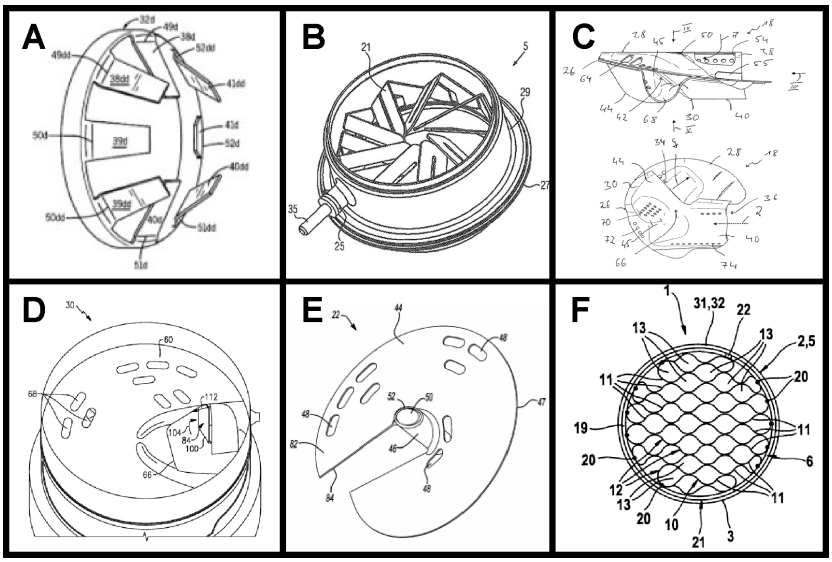

Figure 1: Several of the existing embodiments; A: Axial tabs Type [10], B: Swirl or Fan Type [8], C: Perforated Tunnel Type [18], D: Septum type [19], E: Intermediate Baffle Type [17], F: Directional Mesh Type [14].

is presumed that due to the rather small size of these elements in comparison to the whole ATS system it is directly assumed that their influence is negligible and considered out of interest for acoustic research. The aim of this paper is providing some evidence about the eventual acoustic importance of mixers, and to explore the ability of usual modeling techniques to reproduce their acoustic effects.

The paper is organized as follows: First, the representative type of mixer chosen for this study is described. Secondly, the experimental techniques used and the related post-processing are briefly described. Then, experimental results of pressure drop and transmission loss are shown and discussed, and consequently those results are used to assess different modeling options suitable for engineering practice. Finally, the main conclusions of the work are pointed out.

2. Subject of study: Fan or Swirl Static Mixer

The static mixer studied within this research, corresponds to the swirl or fan type mixer used within the prototype aftertreatment system shown in Figure 2(a). This ATS, consists of a port for DEF injection, followed by the mixer element, a straight pipe section intended to allow for fluid and gas mixing, and two cans containing two and one monolithic catalyst bricks respectively. As it can be seen in Figure 2(b), this mixer does not have a hole opening in the center (contrary to the more extended designs) and has 16 vanes/blades with a certain

twist and orientation that divides the flow and forces spinning, which in turn rises the turbulence and favors the mixing.

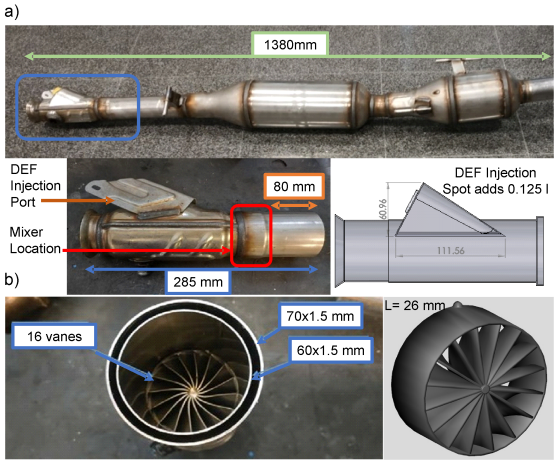

Figure 2: (a) Detail of the device where the mixer element is included; (b) Detail of the mixer studied

3. Experimental Methodology

The following paragraphs summarize the methodologies and facilities used for the pressure drop and transmission loss measurements, and the particular post-processing used in the second case.

3.1. Pressure Drop Measurement

The pressure drop characterization of the device is performed in a flow test rig. The tests were performed in impulsion conditions and with cold flow, being the temperature close to room conditions. The mass flow is provided by a Roots compressor regulated by a PID controller that sets the target mass flow. The maximum mass flow provided by the compressor is between 800-850 kg/h depending on the pressure drop induced by the device installed between the settling tank and the discharge to the atmosphere.

Downstream of the compressor a settling tank of large volume suppresses any residual pulsations from the blower and homogenizes the flow to avoid disturbances in the measurement. The instrumentation at the tank provides the stagnation pressure of the fluid and its temperature, which is necessary to compute the gas density. The difference between the stagnation pressure inside the tank and the atmospheric pressure provides the stagnation pressure drop of the device together with that taking place in the inlet and outlet ducts. Straight ducts with a minimum length of ten times the respective diameter are installed at the inlet and outlet of the tested device, and their pressure drop is obtained

from a separate measurement and then subtracted in order to characterize the device alone. The details of the procedure can be found in [24].

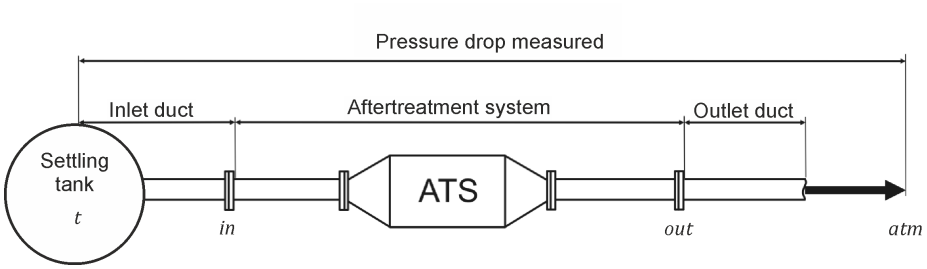

Figure 3: Pressure drop measurements are performed as indicated in this figure, and also for the inlet duct alone

3.2. Transmission Loss Measurement

The experimental set-up used, together with an illustration of the measurement principle, is depicted in figure 4. Two main parts may be distinguished: the pulse generation system and the ducting for pulse propagation and measurement [25], and the mean flow supply. These two systems are briefly described in the following.

Regarding the pulse generation and propagation system, the element is excited by means of a pressure pulse generated by using an electrovalve that controls the discharge from a high-pressure tank. The amplitude and the duration of the pulse can be controlled by modifying the tank pressure and the opening time of the valve such that a substantially flat spectrum is achieved, thus ensuring a proper excitation at all the relevant frequencies.

As the generated pulse propagates down the pipe (wave paths are indicated in the figure by dashed lines) instantaneous pressure is measured with piezoelectric transducers at three different points: midway between the electrovalve and the element (transducer 0), just upstream of the element (transducer 1), and downstream of the element (transducer 2). The duct lengths between the valve and the first transducer and between the third transducer and the last reflecting boundary were chosen so as to enable the isolation of the pressure pulses in the time domain at transducers 0 and 2, and thus the pressure recorded by transducer 3 gives directly the pulse transmitted by the element. The pulse incident to the element is obtained by removing the element itself and measuring the resulting pulse at transducer 2 [25].

The required steady air mass flow is supplied by a Roots compressor driven by an electrical motor connected to the voltage source through a frequency converter, allowing for the automatic control of the mass flow through the element studied. A 30 liter expansion chamber is located downstream of the compressor in order to reduce the pressure fluctuations generated by the blower. The stabilized mass flow is conveyed through a 110 mm diameter pipe up to a hot

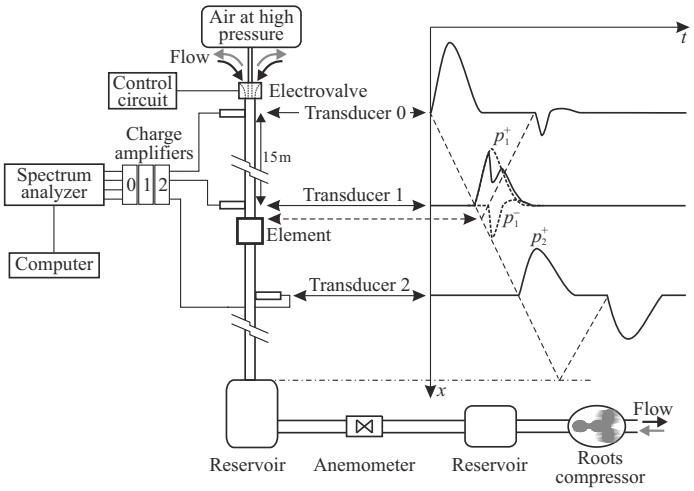

Figure 4: Scheme of the impulse test rig for TL measurement

film anemometer, where the mass flow rate is measured. A 200 liter volume is placed six diameters downstream of the anemometer in order to ensure stagnation conditions downstream of the flow meter. The tank outlet provides the last reflecting boundary to the pulse propagating within the ducting.

In Figure 5(a) an example of the recorded incident and transmitted pulses is shown in the time domain: it is apparent that the pulses are directly isolated without the need for any additional windowing or any other processing.

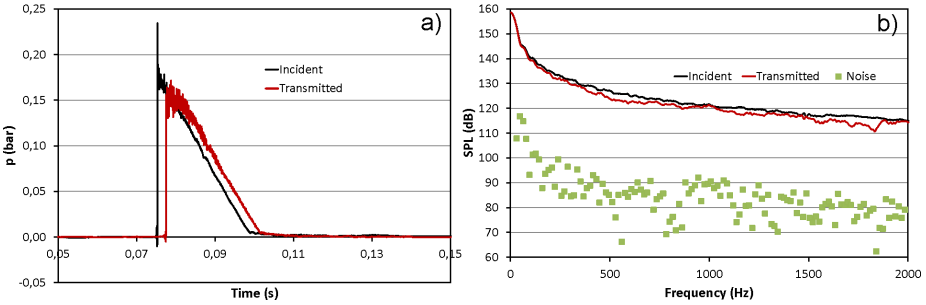

Figure 5: Incident and Transmitted Pulses: (a) time domain; (b) frequency domain, including the transducer background noise

The transducers used for these measurements are Kistler 7001 transducers. The sound pressure level spectra of the incident pulse, of the transmitted pulse and of the background noise signal are shown in Figure 5(b), confirming that the incident spectrum is essentially flat and smooth, as it should be, and that the spectrum of the transmitted wave is well above that of the background noise. It

can be observed that the differences between the incident and the transmitted spectra are relatively small, but still above the sensitivity of the transducers used.

Denoting the spectrum of the incident wave as P_1^+ and the spectrum of the transmitted wave as P_2^+, then one immediately can compute the transmission coefficient T, defined as

$$T = \frac{P_2^+}{P_1^+} \tag{1}$$

Now, from the definition of transmission loss as the ratio of the incident power W_{inc} to the transmitted power W_{tra}, one has:

$$\mathrm{TL} = 10 \log_{10} \frac{W_{inc}}{W_{tra}} \tag{2}$$

The expressions of the power are [26]:

$$W_{inc} = \frac{S_1}{\rho c} \left|P_1^+\right|^2 (1 + M_1)^2 \;\; ; \;\; W_{tra} = \frac{S_2}{\rho c} \left|P_2^+\right|^2 (1 + M_2)^2 \tag{3}$$

where S represents the cross-sectional area, ρ is the density, c is the speed of sound and M is the Mach number. Substituting and rearranging one readily gets:

$$\mathrm{TL}(f) = 20 \log_{10} \left|\frac{1}{T}\right| + 10 \log_{10} \frac{S_1}{S_2} + 20 \log_{10} \frac{1 + M_1}{1 + M_2} \tag{4}$$

Obviously, in the case that the upstream and downstream diameters coincide only the first term in the right-hand-side survives, if one assumes an incompressible mean flow so that $M_1 = M_2$.

The device was measured without any mean flow with a standard pulse in both the direct and the inverse position (in order to allow for the estimation of the transfer matrix), and with three different superimposed mean flows in the direct position, in order to determine the eventual effect of the flow on the attenuation.

3.3. Decomposition Analysis

This analysis [27] is based on the decomposition of the transmission loss into a reflective part and a dissipative part. Consider an aftertreatment device, subject to an upstream excitation and with an anechoic termination at the downstream side (this is the actual situation in the experimental setup used). The power balance may be expressed by stating that the difference between the acoustic power upstream of the device and that downstream is the power dissipated at the device. According to Morfey [26] this can be expressed as:

$$\frac{S_1}{\rho c} \left[\left|P_1^+\right|^2 (1 + M_1)^2 - \left|P_1^-\right|^2 (1 - M_1)^2\right] = \frac{S_2}{\rho c} \left|P_2^+\right|^2 (1 + M_2)^2 + W_{dis} \tag{5}$$

whereW_{dis} is the power dissipated, and P_1^- is the spectrum of the backwards wave component upstream of the device, that is not a direct output of the measurement method used. However, as indicated in [25], it can be estimated with sufficient confidence from the incident pulse and from the pulse recorded by transducer 1 in the presence of the device, that comprises both the incident and the reflected pulses, making use of the following gas-dynamic relation:

$$\left(\frac{p_1(t)}{p_0}\right)^{\xi} = \left(\frac{p_1^+(t)}{p_0}\right)^{\xi} + \left(\frac{p_1^-(t)}{p_0}\right)^{\xi} - 1 \tag{6}$$

where $p_1^+(t)$ and $p_1^-(t)$ are the time-domain counterparts of P_1^+ and P_1^-, respectively, $\xi = (\gamma - 1)/(2\gamma)$, γ being the ratio of specific heats, and p_0 is a reference pressure, typically the pressure of the unperturbed medium. Now, identifying the reflected power as

$$W_{ref} = \frac{S_1}{\rho c} \left|P_1^-\right|^2 (1 - M_1)^2 \tag{7}$$

the balance equation can be written as:

$$1 = \frac{W_{ref}}{W_{inc}} + \frac{W_{tra}}{W_{inc}} + \frac{W_{dis}}{W_{inc}} \tag{8}$$

However, in order to characterize the dissipative behaviour of the device it is preferable to compare the actual power transmitted by the system to the transmitted power in the absence of dissipation. In that case, setting $W_{dis} = 0$ gives for the power transmitted with no dissipation W_{tra}^{ND}:

$$\frac{W_{tra}^{ND}}{W_{inc}} = 1 - \frac{W_{ref}}{W_{inc}} \tag{9}$$

and the aforementioned ratio would thus be

$$\frac{W_{tra}^{ND}}{W_{tra}} = \frac{W_{inc}}{W_{tra}} \left(1 - \frac{W_{ref}}{W_{inc}}\right) \tag{10}$$

Substituting the expression of the incident and the reflected powers one can thus write

$$\frac{W_{tra}^{ND}}{W_{tra}} = \frac{W_{inc}}{W_{tra}} \left[1 - \frac{\left|P_1^-\right|^2 (1 - M_1)^2}{\left|P_1^+\right|^2 (1 + M_1)^2}\right] \tag{11}$$

Now, introducing the reflection coefficient, defined as:

$$R = \frac{P_1^-}{P_1^+} \tag{12}$$

gives

$$\frac{W_{tra}^{ND}}{W_{tra}} = \frac{W_{inc}}{W_{tra}} \left[1 - |R|^2 \frac{(1 - M_1)^2}{(1 + M_1)^2}\right] \tag{13}$$

In logarithmic form, one has

$$10\log_{10}\frac{W_{tra}^{ND}}{W_{tra}} = 10\log_{10}\frac{W_{inc}}{W_{tra}} + 10\log_{10}\left[1-|R|^2\,\frac{(1-M_1)^2}{(1+M_1)^2}\right] \tag{14}$$

and denoting the left hand side as the dissipative contribution to transmission loss, TL_{dis}, and recalling the actual definition of the transmission loss TL as given in equation (2), one can write:

$$\mathrm{TL}_{dis} = \mathrm{TL} + 10\log_{10}\left[1-|R|^2\,\frac{(1-M_1)^2}{(1+M_1)^2}\right] \tag{15}$$

Interpretation of the previous equation in the light of the overall power balance suggests that the second term in the right hand side should be related to the reflective contribution to transmission loss, TL_{ref}, so that this could be defined as:

$$\mathrm{TL}_{ref} = -10\log_{10}\left[1-|R|^2\,\frac{(1-M_1)^2}{(1+M_1)^2}\right] \tag{16}$$

and therefore

$$\mathrm{TL} = \mathrm{TL}_{ref} + \mathrm{TL}_{dis} \tag{17}$$

The expression of the dissipative contribution can be written explicitly in terms of the transmission and reflection coefficients making use of the expression of transmission loss given by equation (4):

$$\mathrm{TL}_{dis} = 10\log_{10}\left[\frac{S_1}{S_2(1+M_2)^2}\frac{1}{|T|^2}\left((1+M_1)^2-|R|^2\,(1-M_1)^2\right)\right] \tag{18}$$

that, in the case of equal diameters upstream and downstream of the device (as it was the case in these particular measurements), assuming again incompressible mean flow so that $M_1 = M_2 = M$, reduces to:

$$\mathrm{TL}_{dis} = 10\log_{10}\left[\frac{1}{|T|^2}\left(1-|R|^2\,\frac{(1-M)^2}{(1+M)^2}\right)\right] \tag{19}$$

4. Experimental results

The following paragraphs cover the results obtained and their analysis. When pertinent, the results for the mixer are shown together with those of the whole aftertreatment device of which it is part, so that a proper context is provided for the evaluation of the importance of any eventual influence.

4.1. Pressure Drop Results

The pressure drop results are shown in figure 6(a). The obtained plot exhibits the expected quasi-quadratic behavior for both the whole device and the mixer element, but with smaller values for the latter, as expected. However, bearing in mind that pressure drop is essentially additive, it is apparent that at medium mass flows the mixer alone accounts for approximately a 20% of the total pressure drop, reaching almost 30% at the maximum mass flow, thus producing a significant increase in backpressure. This is the logical consequence of the operation principle of the device that, as commented in the introduction, promotes mixing essentially by increasing locally the turbulence levels at the wake of the blades.

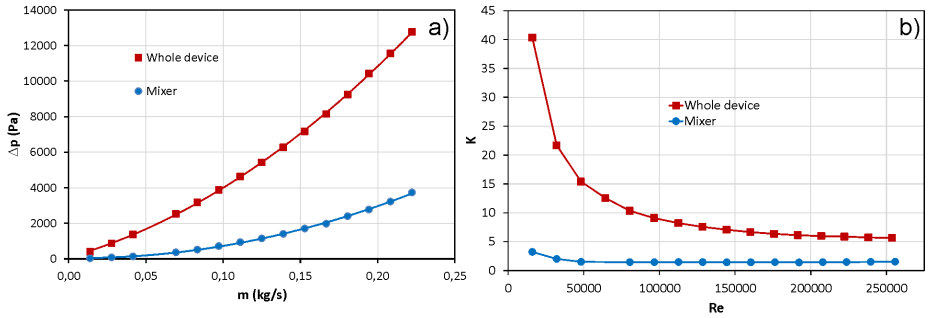

Figure 6: Steady flow characterization: (a) Pressure drop; (b) pressure drop coefficient

Consistently with these results, the pressure drop coefficient (i.e. the ratio of the pressure drop to the upstream dynamic head) plotted in Figure 6(b) as a function of the Reynolds number, exhibits a substantial decrease in value when compared with that of the whole device. Again, the measurements exhibit the right asymptotic behavior within the measurement uncertainties, and it appears that stable fully developed flow conditions have been reached at high Reynolds numbers in both cases.

4.2. Transmission Loss Results

Figure 7(a) shows the comparison between the transmission loss of the whole aftertreatment device and that of the mixer element. Apparently, the contribution of the mixer is relatively small; however, since transmission loss is not an additive magnitude such a consideration could lead to an erroneous judgement on its eventual importance. This statement is justified by the third curve shown, that corresponds to the aftertreatment device without the mixer element: it is apparent that for frequencies below 200 Hz the influence of the presence of the mixer is virtually negligible, but it produces a significant increase in attenuation for frequencies between 200 Hz 700 Hz. Therefore, while the attenuation of the mixer alone is certainly small, it seems necessary to characterize it in

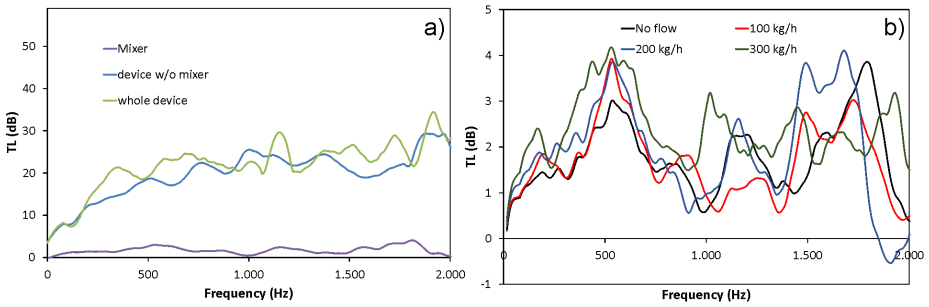

Figure 7: (a)Comparison of the TL of the whole device, the mixer and the rest of the whole device, with no superimposed mean flow; (b) Effect of a superimposed mean flow on the transmission loss of the mixer

order to account for any effects occurring when it is coupled to the rest of the aftertreatment system.

The effect of the flow on the attenuation produced by the mixer alone is shown in Figure 7(b). As it could be expected, both convective (with a certain shift in the characteristic frequencies) and dissipative (with a noticeable increase in the attenuation level at low to medium frequencies) effects are observed.

While in all the cases the attenuation remains very low, it is remarkable that at one of the mass flows considered (namely at 200 kg/h) there is a frequency interval with negative transmission loss, that should be interpreted as sound generation inside the device. In fact, the particular geometry of the mixer considered appears to be susceptible of giving rise to turbulent noise generation due to the turbulent mixing in the wake downstream of the device. The fact that the occurrence of negative TL depends on the value of the mean flow may suggest that this is a Strouhal-governed phenomenon. In order to gain insight into this potentially relevant flow-related feature, the transmission loss decomposition methodology described in paragraph 3.3 was applied, and some relevant findings will now be discussed.

The decomposition at 200 kg/h is shown in Figure 8(a), where it can be observed that, while the reflective transmission loss is relatively smooth and always positive, the dissipative transmission shows a more oscillating behaviour and, more remarkable, becomes negative at some frequencies. Therefore, one could interpret that also in this case there should be some flow noise generation at those frequency bands, but the effect is masked by the reactive effects. However, it is apparent that around 1900 Hz the TL becomes negative and this is uniquely associated with the negative value of the dissipative TL.

If there is actually some flow noise generation, a first guess would be to consider some Strouhal-number-related phenomenon that appears for sufficiently high mass flows. As for higher mass flows such effects should appear at higher frequencies, the frequency axis has been extended in the decomposition representation at 300 kg/h shown in Figure 8(b).

It can be observed that the frequency at which the transmission loss becomes

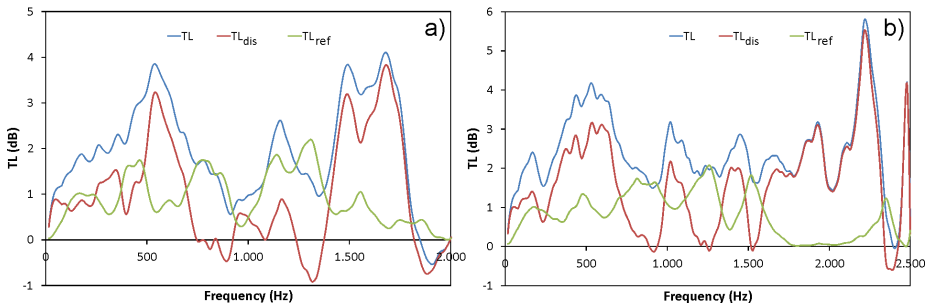

Figure 8: Decomposition of the TL results: (a) 200 kg/h; (b) 300 kg/h

negative is actually shifted to higher values; however, the value obtained (2400 Hz) does not correspond to the same Strouhal number as that observed at 200 kg/h, and thus the results are not totally conclusive. Even so, there are clear indications that flow-noise generation may be taking place at the mixer and, although it is likely that when considering the whole aftertreatment system this will be attenuated by the different elements located downstream and will not reach the tailpipe, there is still a potential for its radiation as shell noise from the duct surface.

5. Modeling study

In order to get further insight into the behavior of the mixer element, different modeling approaches were checked. As an overall reference, a full three-dimensional model of the mixer was built. This was first checked in steady flow, and the results are shown in Figure 9. The streamline representation in Figure 9(a) corresponds to a mass flow of 0.085 kg/s and illustrates the complexity of the flow downstream of the device that, as commented above, is an unavoidable consequence of the primary function of the device. It can also be observed that the DEF injection cavity produces only a small local disturbance in the flow pattern upstream of the mixer. Regarding the computational results for the pressure drop, shown in Figure 9(b), good agreement with the experimental results is observed, with a certain tendency to underestimate the pressure drop at the highest mass flows. However, this provides sufficient confidence on the acoustic results.

The transmission loss was computed by solving the Helmholtz equation in the absence of flow, making use of a standard finite element method, and comparison of the results obtained with the experimental transmission loss is shown in Figure 10(a), where again the transmission loss of the whole aftertreatment device is included as a reference. It can be observed that, while the computational results may be regarded as acceptable, all the more if the low attenuation values are considered, there are some significant differences in the low frequencies, in which the computation underestimates the measured values. It is also

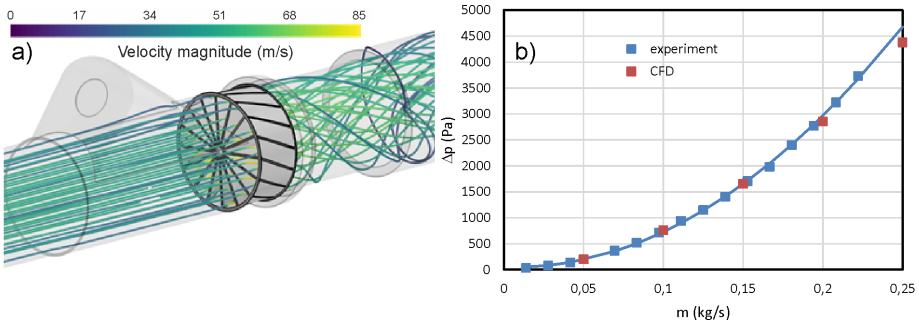

Figure 9: Steady flow in the mixer: (a) streamlines; (b) comparison with experimental pressure drop.

apparent that the computation reproduces the resonance spike occurring at about 2300 Hz. Such a spike can only be the result of a side resonator effect, and this is confirmed in the sound pressure level distribution shown in Figure 10(b): a complex lateral pattern is established in the DEF injection cavity at that frequency, giving rise to a substantial reduction in the sound pressure level at the inlet of the mixer vanes.

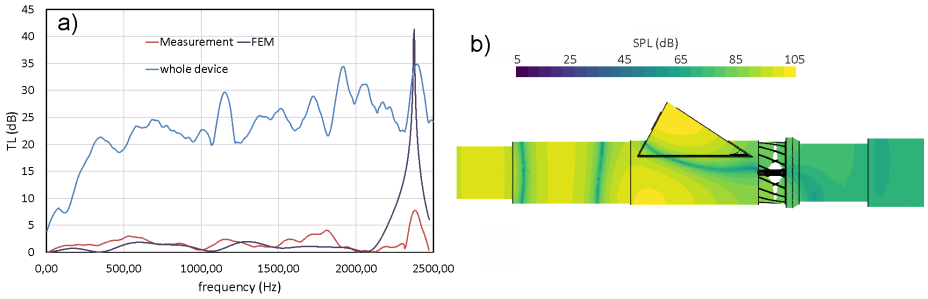

Figure 10: (a) Comparison of measured and computed transmission loss; (b) sound pressure level distribution at the resonance frequency

In this extended representation it is apparent that that resonant spike is influencing the transmission loss of the whole aftertreatment device, which would indicate an approximately additive behaviour that is consistent with the fact that the attenuation of the rest of the system at those frequencies is essentially dissipative [28]. This frequency is in the limit of what would be considered in practice as the relevant frequency range for exhaust design, and therefore in some cases it might be necessary to incorporate this issue into the design process in order to achieve a proper description of the exhaust acoustics. In the frame of one-dimensional models, this would imply using a quarter wave resonator with the same resonance frequency to simulate the effect of the DEF injection volume, while keeping the volume as close as possible to the real one,

so that the low frequencies are not severely affected.

Regarding the differences observed in the low frequencies, they should be attributed to the dissipative effects caused by the presence of the vanes, effects that are not accounted for by the numerical model used. That this is the case can be evidenced in several ways. One possibility is checking the elements of the computed transfer matrix against those of the measured transfer matrix, which can be obtained from the direct and reverse transmission and reflection coefficients [28], as represented in Figure 11 for the matrix elements T_{11} and T_{12}.

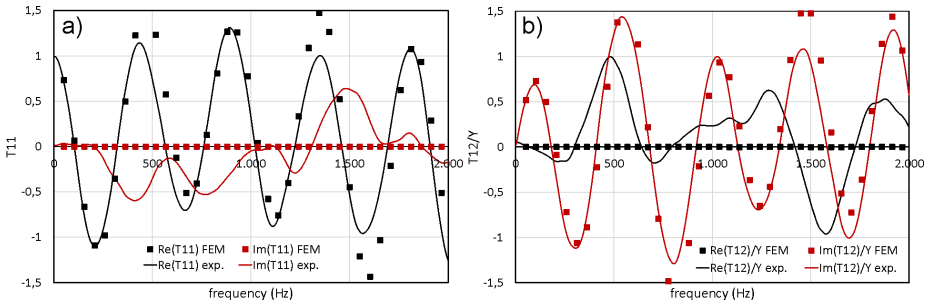

Figure 11: Comparison of measured and computed transfer matrix elements: (a) T_{11} (b) T_{12}/Y_0, where Y_0 is the characteristic impedance of the duct

It can be observed that, while for the real part of T_{11} and the imaginary part of T_{12} the computational results reproduce the overall tendency seen in the experimental values, even if with some local differences in the amplitude of he oscillations, the computed imaginary part of T_{11} and real part of T_{12} are zero, whereas non-zero values are found in the experimental results. Having $\mathrm{Re}(T_{11}) = \mathrm{Im}(T_{12}) = 0$ is a characteristic of conservative systems [28], i.e. an indicator of the absence of dissipation. The fact that $\mathrm{Re}(T_{11}) \neq 0$ and $\mathrm{Im}(T_{12}) \neq 0$ indicates that there is a significant dissipation in the measured values, and thus that this is the origin of the deviations observed in the transmission loss.

Additional support for this statement may be obtained by again making use of the transmission loss decomposition. If one compares the reflective contribution TL_{ref} for the no-flow case with the computational results for the TL one gets the results shown in Figure 12. As it can be observed, the computational results are closer to those of TL_{ref} than to those of the full transmission loss, not only in the values but also in the low frequency tendencies. Additionally, it may be seen that, as expected, the effect at the resonance frequency is correctly attributed by the transmission loss decomposition to reactive effects, which provides additional confidence in the ability of the method proposed in [27] to identify reactive and dissipative contribution to attenuation.

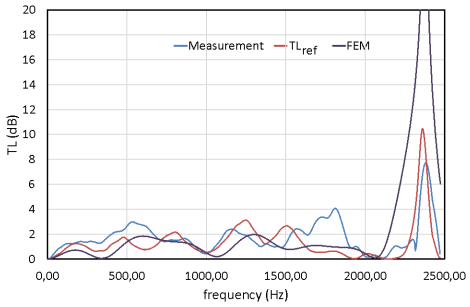

Figure 12: Comparison of measured and computed transmission loss, including the reflective contribution TL_{ref}

6. Summary and conclusions

A comprehensive set of pressure drop and transmission loss measurements were performed on a representative static mixer device complementary to DEF injection in an aftertreatment system. The experimental procedures were briefly described, with some more detail in the less conventional decomposition of the TL into a reflective and a dissipative part.

Regarding the pressure drop results, they match the expected behavior, both in terms of the asymptotic trend of the pressure drop coefficient at high Reynolds numbers, and of the dependence of the pressure drop on the mass flow. The mixer contribution to the overall pressure drop of the whole aftertreatment system is not negligible, which is reasonable in view of its operation principle based on turbulent mixing.

Regarding the transmission loss results, it has been observed that, while the attenuation produced by the mixer alone is indeed small, it produces a non-negligible effect when coupled to the rest of the aftertreatment system, most likely due to the presence of dissipative terms, and therefore its presence should not be ignored in principle. The effect of the flow on the transmission loss of the mixer alone exhibited both the convective and dissipative effects expected but, additionally, the flow caused the occurrence of negative transmission losses, which indicate some flow noise generation in the device (which might be expectable in view of its geometry) that may require special care in the mechanical design of the connection to the aftertreatment system.

This negative transmission loss was further analyzed in terms of the decomposition into a reflective and a dissipative contribution, showing that the negative TL is directly related with negative values of the dissipative term, but also that the dissipative term becomes negative even in cases where the total TL is positive, indicating that in those cases the sound generated must be attenuated at the device itself. While the results were not fully conclusive in terms of a clear dependence on the Strouhal number, a certain dependence of the occurrence of negative TL with the flow was found.

Finally, a three-dimensional model was used in order to shed additional light onto the experimental results. From this work, it has been possible to identify the resonant effect of the DEF injection cavity, and the overall importance of dissipative effects in the attenuation of the device, even at low frequencies. Both aspects may pose non-negligible challenges in the development of simple one-dimensional models useful in exhaust design.

7. Acknowledgments

This paper is derived from the research activities developed during the doctoral studies of co-author Alvaro Redondo, which included the characterization of the ATS where the mixer element was located; all his research was supported by the Universitat Politècnica de València (UPV) through the Programa de Ayudas de Investigación y Desarrollo PAID-01-19 which grants him a predoctoral contract.

References

[1] P. Chen, J. Wang, Nonlinear model predictive control of integrated diesel engine and selective catalytic reduction system for simultaneous fuel economy improvement and emissions reduction, Journal of Dynamic Systems, Measurement, and Control 137 (8).

[2] D. W. Kapsos, C. D. Bremigan, M. P. Adams, P. M. Klein, Exhaust aftertreatment system with spiral mixer (U.S. Patent 7712305, May. 2010).

[3] G. Mehdi, S. Zhou, Y. Zhu, A. H. Shah, K. Chand, Numerical investigation of SCR mixer design optimization for improved performance, Processes 7 (3) (2019) 168.

[4] L. Tan, P. Feng, S. Yang, Y. Guo, S. Liu, Z. Li, CFD studies on effects of SCR mixers on the performance of urea conversion and mixing of the reducing agent, Chemical Engineering and Processing-Process Intensification 123 (2018) 82–88.

[5] J. Michelin, F. Guilbaud, A. Guil, I. Newbigging, M. Jean, M. Reichert, Balenovic, Advanced compact SCR mixer: Bluebox, SAE Technical Paper 2014-01-1531 (2014).

[6] M. Chen, S. Williams, Modelling and optimization of SCR-exhaust aftertreatment systems, SAE Technical Paper 2005-01-0969 (2005).

[7] S. Tummala, A. Dimopoulos, Mixer for after-treatment system (G.B. Patent 2550173, Nov. 2017).

[8] T. Gschwind, Mixer for aftertreatment of exhaust gases (U.S. Patent 0315943 A1, Nov. 2015).

[9] P. M. Cornaglia, G. Villata, Static mixer for the treatment of exhaust gases and manufacturing method thereof (U.S. Patent 8956040, Feb. 2015).

[10] C. R. Cheng, T. E. Page, Exhaust aftertreatment mixer with stamped muffler flange (U.S. Patent 7533520, May 2009).

[11] C. Paterson, D. B. Mastbergen, Low pressure drop mixer for radial mixing of internal combustion engine exhaust flows, combustor incorporating same, and methods of mixing (U.S. Patent 8459017, Jun. 2013).

[12] Y. J. Cho, J. W. Park, Static mixer or mixing urea aqueous solution and engine exhaust gas (U.S. Patent 0104531 A1, May. 2013).

[13] Z. G. Liu, M. T. Zuroski, C. D. Bremigan, K. J. Kicinski, C. R. Cheng, Exhaust aftertreatment device, including chemical mixing and acoustic effects (U.S. Patent 6722123, Apr. 2004).

[14] G. Wirth, F. Neumann, Static mixer and exhaust gas treatment device (U.S. Patent 7793494, Sep. 2010).

[15] Y. Yi, J. Sun, SCR reductant mixer (U.S. Patent 8359832, Jan. 2013).

[16] H. Gentgen, Static mixer for an exhaust gas system of an internal combustion engine (U.S. Patent 8801267, Aug. 2014).

[17] J. Denton, Dual auger mixing system (U.S. Patent 0243510 A1, Aug. 2016).

[18] E. Kurpejovic, K. K. Vempati, V. B. Solipuram, Mixer (U.S. Patent 0226379 A1, Jul. 2019).

[19] E. Alano, J. Scott, Mixer with swirl box for a vehicle exhaust system (WO Patent 012829 A1, Jan. 2015).

[20] J.-W. Seo, K.-I. Lee, J.-T. Oh, Y.-H. Choi, J.-H. Lee, J.-I. Park, The study on the effects of mixer configurations on fluid mixing characteristics in SCR systems, Transactions of the Korean Society of Automotive Engineers 16 (6) (2008) 192–199.

[21] C. Zhang, C. Sun, M. Wu, K. Lu, Optimisation design of SCR mixer for improving deposit performance at low temperatures, Fuel 237 (2019) 465–474.

[22] A. Blinov, N. Malastowski, A. Bykov, Performance evaluation of static mixers in the urea injection pipe for SCR systems, in: International Conference on Industrial Engineering, Springer, 2019, pp. 1465–1473.

[23] C. Zhao, D. Lou, Y. Zhang, K. Lu, S. Liu, Application study on a new hybrid canning structure of after-treatment system for diesel engine, Energies 13 (3) (2020) 734.

[24] A. J. Torregrosa, J. R. Serrano, F. J. Arnau, P. Piqueras, A fluid dynamic model for unsteady compressible flow in wall-flow diesel particulate filters, Energy 36 (1) (2011) 671–684.

[25] F. Payri, J. M. Desantes, A. Broatch, Modified impulse method for the measurement of the frequency response of acoustic filters to weakly non-linear transient excitations, Journal of the Aoustical Society of America 107 (2) (2000) 731–738.

[26] C. L. Morfey, Sound transmission and generation in ducts with flow, Journal of Sound and Vibration 14 (1) (1971) 37–55.

[27] R. Kabral, F. Auriemma, M. Knutsson, M. Åbom, A new type of compact silencer for high frequency noise, in: 9th International DAAAM Baltic Conference, Danube Adria Association for Automation and Manufacturing, 2014, pp. 29–35.

[28] A. J. Torregrosa, P. Piqueras, E. J. Sanchis, S. Guilain, M. Dubarry, Assessment of acoustic reciprocity and conservativeness in exhaust aftertreatment systems, Journal of Sound and Vibration 436 (2018) 46–61.